Successful amino-grafting functionalization of MIL-53(Al) through impulse dielectric barrier discharge plasma for hydrogen storage

A. NAJAH[1,] , R. JEAN-MARIE-DESIREE[1], D. BOIVIN[1], R. LUAN SEHN CANEVESI[2], C. NOËL[1], M.T. IZQUIERDO[3], A. CELZARD[2,4], V. FIERRO[2], L. DE POUCQUES[1], G. HENRION[1], S. CUYNET[1]*

[1] *Université de Lorraine, CNRS, IJL, F-54000 Nancy, France*

[2] *Université de Lorraine, CNRS, IJL, F-88000, Épinal, France*

[3] *Instituto de Carboquímica (ICB-CSIC), E-50018, Zaragoza, Spain.*

[4] *Institut Universitaire de France (IUF), F-75231, Paris, France*

Corresponding author : *aymane.najah@univ-orleans.fr*

ORCID ID**: **0000-0002-7545-8388

Keywords: *Plasma functionalization; IDBD; MIL-53(Al); NH_3; hydrogen storage.*

Abstract:

The present study investigates the functionalization of a commercial Metal-Organic Framework (MOF) named "MIL-53(Al)" using an NH_3 impulse dielectric barrier discharge (IDBD) plasma treatment. The main objective of this research is to assess the efficacy of the IDBD treatment in grafting nitrogenous groups onto the MOF's organic ligand. Additionally, the impact of the plasma functionalization on the hydrogen adsorption capacities of the "MIL-53(Al)" after IDBD treatment is also studied. In order to accomplish these objectives, plasma diagnostics and comprehensive material characterization techniques are utilized. Structural and thermal analysis by HT-XRD and TGA-MS respectively, indicate the excellent thermal and chemical stability of the material against high temperatures and ammonia. Chemical analysis of the materials by XPS shows that the IDBD treatment effectively functionalizes the MIL-53(Al) by substituting a carbon with a nitrogen within the organic

ligand. Finally, the analysis of the hydrogen adsorption capacities at 1 bar and 25 °C reveals that the amount of hydrogen stored in the MIL-53(Al) treated by IDBD is significantly higher. Specifically, the amount of hydrogen stored surpassed the untreated MIL-53(Al) by approximately 50%.

1. Introduction

Metal-Organic Frameworks (MOFs) are hybrid crystalline porous materials, consisting of metal ions or clusters connected through organic ligands by coordination bonds. These compounds have received much attention due to their high specific surface area and pore volume[1-5]. MOFs have shown high promise for many practical and industrial applications, such as gas storage and separation[6-10], catalysis[11-14], drug delivery[15-17], energy[18-21], etc. Despite these numerous application fields, particularly in gas storage, their performance still requires some improvements to achieve higher adsorption capacities at standard temperature and pressure.

Thereby, various strategies have been explored to optimize MOF structures to improve gas adsorption capacities, e.g. H_2 adsorption[22-26]. Among these methods, MOFs functionalization has been proved experimentally and computationally that it is an effective approach for performance optimization. Functionalization is achieved mainly by grafting functional groups (*e.g.* -Cl, -Br, $-NH_2$, etc.) onto MOF' organic ligand. This can be done either during MOF synthesis process (pre-functionalization)[27-29], or carried out after MOFs synthesis (post-synthetic modification)[30-32]. Zhang et al.[33] studied 24 MOF-177 structures with different functional groups on the benzenetribenzoate (BTB) ligand. Their study has shown that mixing of functionalities (-H, $-NH_2$ and $-C_4H_4$) is an efficient strategy to enhance the H_2 uptake by 25%. Xia et al.[31] investigated the effect of functional groups on the H_2 storage properties of MOF-808-X (X= -OH, $-NO_2$, $-CH_3$, -CN, -I). The simulation of H_2 uptakes and the isosteric heat of adsorption at -196°C showed that all these functional groups have a favorable effect on H_2 adsorption, and that the -CN group is the most promising to improve H_2 uptake.

In general, MOFs functionalization is carried out via wet-chemical methods, which often involve the use of solvents and liquids in the process. In a previous paper[34], we evoked the possibility to functionalize these compounds by using low temperature plasma treatments. These latter are widely used to modify surface properties of some materials, *e.g.* polymer[35-37], cotton[38-40], metal and alloy[41-43], etc. As a dry chemical method, plasma treatment turns out to be a less harmful and an eco-friendlier process compared to conventional chemical ones. During plasma functionalization, reactive gas molecules are dissociated, generating energetic species that are accelerated towards the material surface within the plasma sheath. The bombardment of the material by these reactive species causes the breaking of some covalent bonds and the formation of free radicals. These radicals then interact

with the active species of the plasma, resulting in functionalization on the surface of the treated material depending on the nature of the gas phase. Moreover, we demonstrated that it is possible to pre-functionalize MOFs organic ligands (terephthalic acid) by grafting amino groups on its aromatic ring via an impulse dielectric barrier discharge (IDBD) plasma treatment[34]. The obtained results suggest that plasma treatments could be useful to synthesize amino based MOFs.

In the present work, we investigate systematically the post-synthetic modification process of a commercial MOF, the MIL-53(Al) (Basolite A100), by using an impulse dielectric barrier discharge plasma treatment. One of the main interesting features about the "MIL class" of metal-organic frameworks relies on their ''breathing effect''[44-46]. This behavior is observed for various external stimuli such as the presence of guest molecules within the pores[47], the variation of gas pressure[47], changes of temperature[47]. Hence, with the presence of one of these stimuli, it involves a flexible-reversible phase transition between narrow pores (n_p) and large pores (l_p) forms, thus making it possible to have an expansion/contraction of the pore volume dimension up to 40% in unit cell volume[45]. Therefore, considering the same experimental protocol used in our previous work on terephthalic acid, the goal of this study is to examine the efficiency of the IDBD treatment to graft nitrogenous groups onto MIL-53(Al) organic ligand. To do so, plasma diagnostics are performed to analyze the plasma phase electrically and optically. In addition, materials characterization is carried out to investigate the grafting process on the MIL-53(Al) after plasma treatment, and on the application side, to examine the H_2 adsorption capacities after IDBD treatment.

2. Experimental setup

2.1. IDBD system and material

The experimental schematic diagram used for the IDBD treatment is depicted in figure 1. The DBD cell comprises two square plane-parallel copper electrodes, both covered with an aluminum nitride dielectric in a typical planar symmetric configuration. The upper electrode is connected to the high voltage, whereas the lower electrode is grounded. More details about the IDBD system used for this study can be found in our previous work[34]. Briefly, the DBD cell is maintained inside a spherical stainless-steel reactor. The experiment is carried out within a static gas inlet regime at a constant pressure of 0.1 bar. This is reached by first evacuating the reactor via a pumping system down to 10^{-9}

bar residual pressure. Then, the reactor is filled in with ammonia gas (Air Liquide, 99.9% purity) to achieve an operating pressure of 0.1 bar. The IDBD treatment is performed in a pulsed regime by using two high voltage generators (Technix SR15-R-1200) connected to a high frequency switcher (BEHLKE HTS 301-03-GSM) that is triggered by a low frequency signal generator (Yokogawa FG120). The material to be treated is placed on the bottom dielectric. For the plasma treatment, the powered electrode is supplied with 6 kV_{p-p} (+3 kV, - 3 kV) high voltage square pulses at a frequency of 4 kHz, for 1 h of treatment, and with 3 mm gap distance between the dielectrics.

The MOF MIL-53(Al) was purchased from the supplier SIGMA ALDRICH (Basolite A100). Initially reported by Férey et al.[48], MIL-53(Al) has a 3D structure build up from chains of octahedral $AlO_4(OH)_2$ units connected through 1,4-benzenedicarboxylate anions (terephthalate), as shown in figure S1 (supporting information). The general description provided by the supplier shows that this material has a BET surface area, A_{BET}, of 1100-1500 $m^2.g^{-1}$, a bulk density of 0.4 $g.cm^{-3}$. Moreover, MIL-53(Al) can be reactivated at 200 °C under vacuum.

In order to consider the possible effect of ammonia gas on the structure of MIL-53(Al), labelled as "MIL-53(Al) untreated", it was treated in two different conditions: i) direct exposition to ammonia gas, and the resulting material was labelled as "MIL-53(Al) expo NH_3"; ii) direct exposition to NH_3 + plasma treatment, and the resulting material was labelled as "MIL-53(Al) IDBD NH_3". Hence, these three materials are compared in this study.

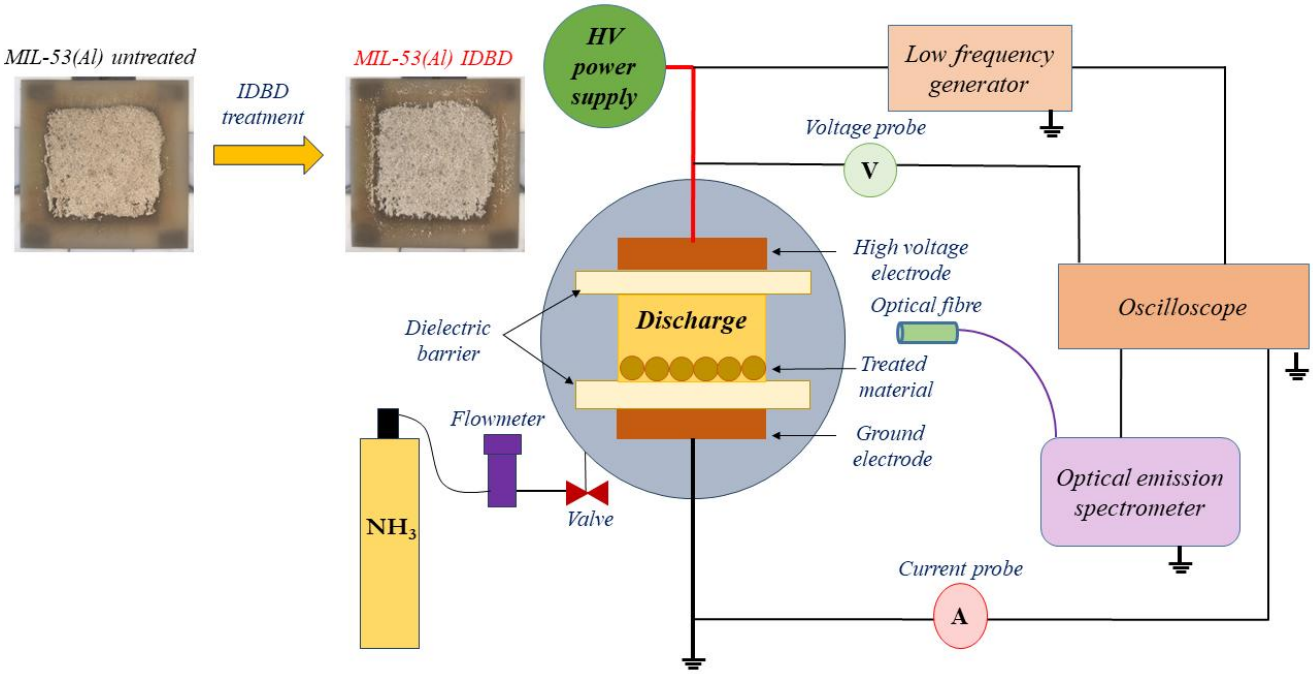

Figure 1. *Schematic diagram of the setup used for the IDBD plasma treatment of MIL-53(Al) with* NH_3.

2.2. Characterization

2.2.1. Plasma diagnostics

- **Electrical measurements**

The electrical parameters of the IDBD discharge were recorded by a voltage probe (Cal Test CT4028, with a bandwidth from DC to 220 MHz) and a current probe (Magnelab CT-D1.0-B, with a bandwidth from 200 Hz to 500 MHz). The two probes are connected to an oscilloscope (LeCroy 104Xi, with an acquisition frequency of 10 Gsa/s and a bandwidth of 1 GHz).

- **Optical emission spectroscopy (OES)**

The chemical species present in the plasma during the IDBD treatment of MIL-53(Al) were determined by optical emission spectroscopy (OES) measurement, with a Jobin-Yvon Triax 550 spectrometer equipped with a 1200 grooves mm^{-1} grating and an intensified charged couple device camera (ICCD). The light emitted by the plasma was collected through a quartz window by an optical fiber fronting the discharge. The emission spectra were recorded between 250 nm and 700 nm, with a spectral resolution of 0.07 nm. The synchronization of the OES measurements with the discharge pulses is detailed in our previous work[34].

2.2.2. Material characterization

- **X-ray diffraction**

The study of the structural behavior of the materials as a function of the temperature was carried out via high temperature X-Ray Diffraction (HT-XRD), using a Panalytical X'Pert Pro MPD diffractometer, with Cu $K_{\alpha 1}$ *(λ =1.5406 Å)* radiation, operated at a voltage of 40 kV and a current of 40 mA, with a high temperature attachment, in θ-θ geometry. The diffraction patterns were recorded over a 2θ range between 5° and 40°, with a scan rate of 4 °/min and a step size of 0.02°. The recording of the diffractograms were carried out under argon atmosphere, at a heating rate of 5 °C min^{-1}, ranging from 50 °C to 600 °C, with a diffractogram recorded every 50 °C. The powder samples were prepared on a refractory pyrophyllite sample holder. The assignation of crystalline phases was performed by using DIFFRACT.EVA software that supports a reference pattern database for phase identification, in our case ICDD powder diffraction file (PDF-4)[49].

- **Thermogravimetric analysis-mass spectrometry (TGA-MS).**

The thermogravimetric measurements, coupled with a mass spectrometer, were carried out using a thermogravimetric analyser (SETARAM Setsys Evolution) and a mass spectrometer (OmniStarGSD301C-Pfeiffer Vacuum). An amount of 15 mg for each sample was prepared in a platinum crucible. The measurements were carried out under a stable helium flow (20 $mL.min^{-1}$), in the temperature range of 20-800 °C, at a heating rate of 5 °C min^{-1}.

- **X-Ray photoelectron spectroscopy (XPS)**

-

The chemical surface analysis of the samples was carried out by a SPECS GmbH X-Ray photoelectron spectrometer, equipped with a non-monochromatized Mg k_α radiation (1253.6 eV) and with an energy analyzer PHOIBOS 150 (MCD-9 detector). The samples were introduced into the analysis chamber where the vacuum was under $6.6.10^{-12}$ bar. The hemispherical electron energy analyzer was operated at pass energy of 50 eV for survey, and 20 eV for high-resolution spectra. The spot size of the analysis is 100 µm. Binding energies (BEs) were referenced to the C_{1s} peak (284.5 eV). Current region sweeps for C_{1s}, O_{1s}, N_{1s} and Al_{2p} were obtained. The CASA data processing software[50] allowed smoothing, background subtraction, peak fitting and quantification.

- **Gas adsorption**

The surface areas of the MIL-53(Al) samples were determined by applying the BET method to the nitrogen (N_2) and argon (Ar) adsorption isotherms in the adequate range of relative pressures (P/P_0)[51]. The N_2 isotherms were performed at -196 °C, whereas Ar isotherms were performed at -186 °C using a fully automatized manometric adsorption unit 3Flex (Micromeritics, Atlanta, GA). The volume uptake at P/P_0=0.97 ($V_{0.97}$, Gurvich volume) was also determined for both gases. Low pressure (up to 1bar) H_2 isotherms were measured at -196 ºC and 0 ºC using the same manometric device as mentioned earlier.

Prior to conducting the adsorption experiments, the samples underwent heating at 110 °C and high vacuum outgassing (reaching a pressure of $1.3.10^{-8}$ bar) for a minimum of 12 h. Following the evacuation process, the pressure was gradually increased up to 1 bar by dosing the selected gas to determine the amount of gas adsorbed as a function of the equilibrium pressure. Temperatures below 0 °C were reached using a single-stage closed-cycle cryogenic refrigerator, while temperatures above 0 °C were obtained using a water bath. More details are given elsewhere[52,53].

3. Results and discussions

3.1. U-I characteristics

The current-voltage characteristics of the IDBD with and without the MIL-53(Al) powder material is shown in figure 2. By observing the voltage waveforms, it appears that the plasma is ignited for a minimal measured voltage applied on the electrodes of $\Delta V \approx 2$ kV. On the other hand, the maximum peak of the discharge current has a duration of $\Delta t = 76$ *ns*. Besides, the absolute current values are different between the positive and the negative polarities in both treatments, this difference in absolute current values was previously discussed[34]. As a reminder, this is first due to the asymmetry of the copper electrodes. The upper one has a square shape while the lower electrode has a typical geometry that allows the sample powder to be confined in the center zone of the dielectric. Secondly, as the powder is placed at the top of the lower dielectric, the mechanism of ignition and maintenance of the plasma according to the reversal of polarity is hence different from the situation where it is only a question of a discharge between two identical dielectrics. Furthermore, it is obvious that there is a remarkable decrease in current values when adding the material "MIL-53(Al)" during the IDBD treatment, and the voltage curves are relatively stable in the two treatments. This behavior can be explained by a variation in the dielectric constant of the system caused by the addition in the DBD cell of an insulating material that acts itself as a dielectric[34]. Thus, this change of the dielectric constant could influence the current evolution of the discharge, but without having a drastic impact on the breakdown conditions of the discharge, as shown in the voltage curves.

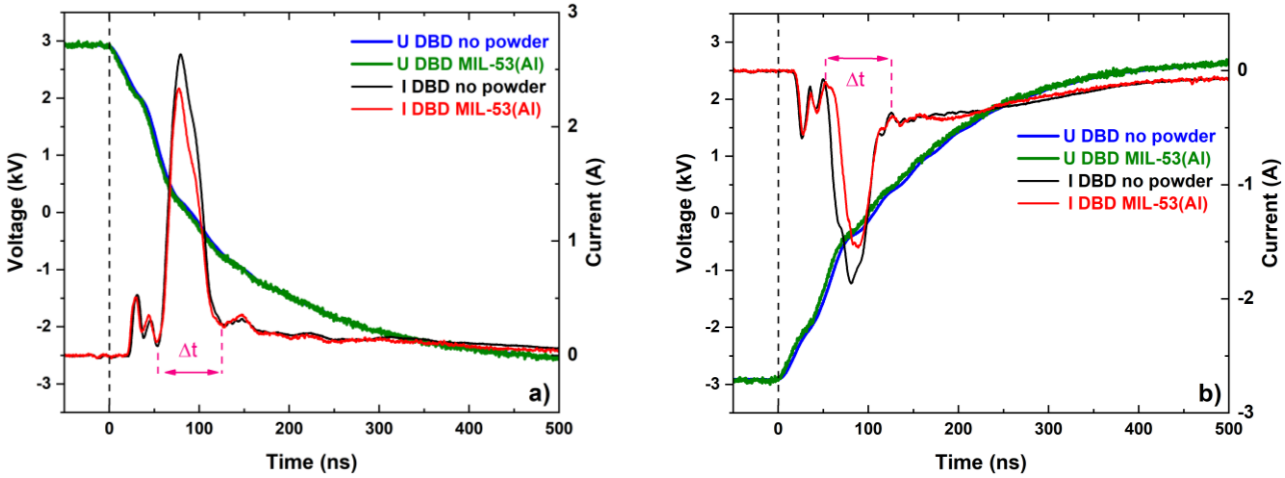

Figure 2. *Current-Voltage measurements of the IDBD plasma treatment of MIL-53(Al) at 6 kVpp*

voltage, pressure of 0.1 bar, frequency of 4 kHz, and 3 mm of interelectrode distance. a) falling edge of the voltage, b) rising edge of the voltage.

3.2. Optical emission spectroscopy (OES)

The emission spectrum obtained during the plasma treatment of MIL-53(Al) is shown in figure 3. It reveals the presence of various atomic and molecular excited species originated from the dissociation of NH_3 molecules. These include the presence of N_2 emission lines belonging to the second positive system $(C^3\Pi_u \rightarrow B^3\Pi_g)$ of molecular nitrogen, with an intense peak at 337 nm, and a peak at 336 nm corresponding to the transition $(A^3\Pi \rightarrow X^3\Sigma^-)$ of NH species. Moreover, other bands and lines are observed; a wide dominant band is observed between 563 nm and 567 nm, which is attributed to the Schutter system of NH_3 molecules[54]. Atomic hydrogen is also detected, with a line at 656 nm, corresponding to the first transition in the Balmer series (H_α). On the other hand, no emission lines (such as Al or C atomic lines or CH, C_2 or CN molecular bands) are observed that could reflect a possible deterioration of the material due to ammonia and/or plasma treatment. This finding may suggest at first sight that MIL-53(Al) is rather stable in NH_3 plasma. However, material characterization of the MIL-53(Al) treated by IDBD process is necessary to determine the effect of the plasma on the material. This is presented in the following sections.

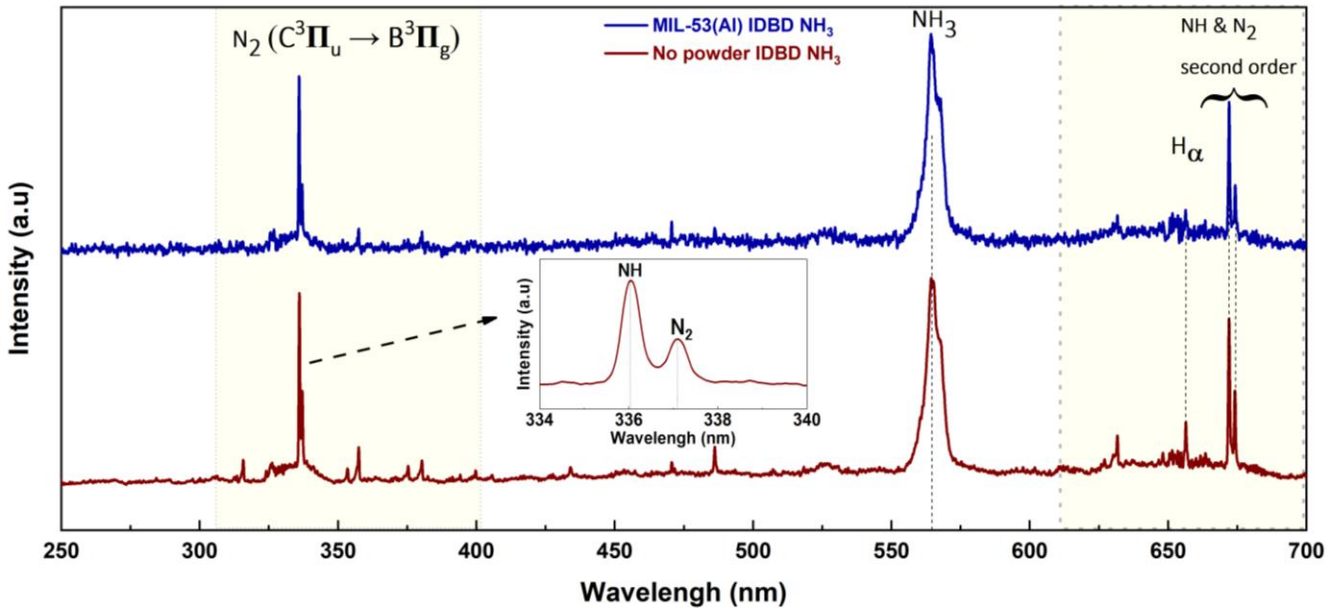

Figure 3. *OES spectrum of an IDBD plasma in NH_3, at 6 kV_{pp} voltage, pressure of 0.1 bar, frequency*

of 4 kHz, and 3 mm of inter-dielectric distance, and an OES spectrum of IDBD plasma with the same discharge conditions but with MIL-53(Al) material/powder.

3.3. High-temperature X-ray diffraction (HTXRD)

High-temperature X-ray diffraction patterns of the three materials, pristine MIL-53(Al), MIL-53(Al) exposed in NH_3 (gas phase only), and MIL-53(Al) treated by IDBD in NH_3, are depicted in figure 4. It is clear that the three materials have the same diffraction peaks, indicating that no structural change occurred following the exposure to NH_3 and the IDBD treatment in NH_3. This seems to confirm the good chemical stability of MIL-53(Al) against ammonia. Indexation of the diffractograms show a mixture of two phases of the crystalline structure of MIL-53(Al). The first phase presented by the diffraction peaks at 2θ = 8.74°, 15.18°, 17.66 °, 25.04°, and 26.57° is attributed to the dehydrated phase of the material[55,56] (PDF 00-067-0849), in this case to the large-pore MIL-53(Al)_l_p that presents an orthorhombic structure. The second phase presented by the diffraction peak obtained at 12.39° corresponds to the hydrated phase of the material with narrow pores[55,56] MIL-53(Al)_n_p (PDF 00-066-1097) that has a monoclinic structure. Thus, the studied structure of MIL-53(Al) exhibits a phase mixture of large and narrow pores. Table S1 (supporting information) presents the lattice parameters of the two phases of MIL-53(Al).

In addition, the diffractograms obtained from the three materials show a remarkable structural stability with the continuous increase in temperature since they maintain their crystalline structure up to 450 °C, a temperature at which almost all the diffraction peaks disappear, except for the two peaks at 25.04° (132) and 26.57° (033). The disappearance of the first main diffraction peaks corresponding to the (020), (101) and (022) planes is an indication of the structural deterioration of the material at this temperature. Beyond 450 °C, the remaining diffraction peaks represent *a priori* the residue in the form of metal oxide. Furthermore, there is a significant increase in the intensity of the main (020), (101) and (022) peaks with increasing temperature, suggesting a possible desorption of water and other solvents used during MIL-53(Al) synthesis. In addition, a small shift of the peaks is observed under the effect of the temperature towards the large angles 2θ for the three MOFs. This behavior could be due to a shrinking of MOFs structures caused by the thermal effect, thus influencing the lattice parameters. As for the hydrated phase of the materials, we can notice that as the temperature rises, the intensity of the

peak at 2θ = 12.39° decreases until it disappears at about 200 °C. Therefore, from 200 °C the material has a single phase with large pores. As a result, the analysis proved that the three materials have the same structure, and the same thermal stability up to 450 °C.

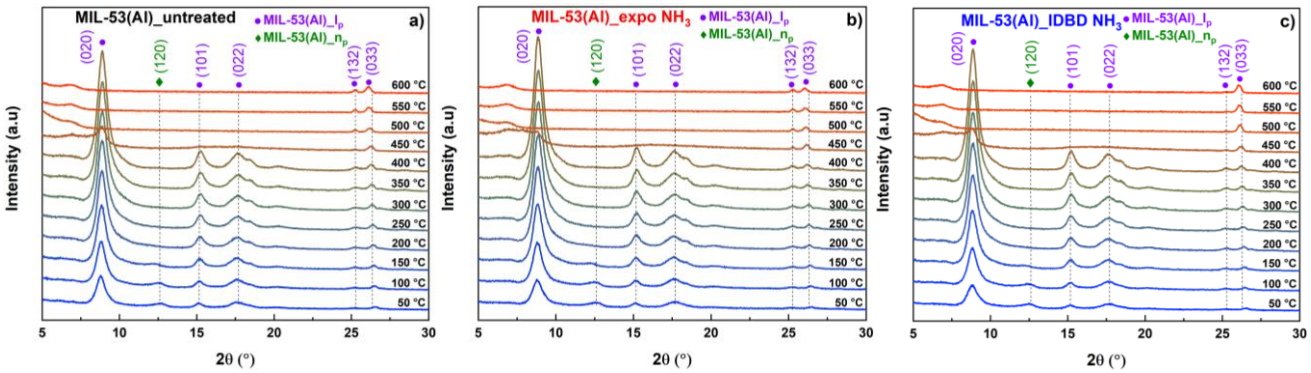

Figure 4. *HTXRD patterns obtained under argon atmosphere between 50 °C and 600 °C of the pristine MIL-53(Al), MIL-53(Al) exposed in NH_3 and MIL-53(Al) treated by IDBD in NH_3*

3.4. TGA-MS analysis

The thermogravimetric analysis of the three materials; pristine MIL-53(Al), MIL-53(Al) exposed to NH_3 and MIL-53(Al) treated by IDBD in NH_3 is presented in figure 5. The three TGA curves (fig. 5.a) show that they have almost the same thermal stability, with decomposition occurring at a temperature between 550 °C and 600 °C. This is in agreement with the results obtained previously by XRD, confirming the good chemical stability of this material against ammonia, and also the good thermal stability of this compound.

The DTG curves of the three materials show two distinct mass losses. The first mass loss, between 100 °C and 400 °C, is relatively low and almost identical for the three materials with losses of 1.7% for the pristine MIL-53(Al) (fig. 5.b), 1.8% for MIL-53(Al) exposed in NH_3 (fig. 5.c) and also for MIL-53(Al) treated by IDBD in NH_3 (fig. 5.d). The origin of this first mass loss on the three materials can be attributed to the degassing of water trapped in the pores, as well as other solvents used during the synthesis of MIL-53(Al) such as dimethylformamide (DMF). Mass spectrometry measurements (fig. 5.b, c, d) show that this first mass loss corresponds to m/z= 18 (H_2O), which correlates with the data obtained by XRD for the hydrated phase, and also to m/z=16 (CH_4), m/z=44 (CO_2) and m/z=78 (C_6H_6), potentially attributed to material activation.

The second mass loss between 450 °C and 670 °C is also similar for the three samples: 52.7% for the reference MIL-53(Al), 54.7% for the MIL-53(Al) exposed in NH_3 and 52.6% for MIL-53(Al) treated by IDBD in NH_3. This second main mass loss is attributed to the decomposition and the collapse of MOFs structure. The thermal decomposition of MOFs gives some aluminum oxide residues. Data collected by mass spectrometry during the second mass loss show detection of signals at m/z=12 (C), m/z=15 (CH_3), m/z=16 (CH_4), m/z = 44 (CO_2) and m/z = 78 (C_6H_6). All these signals confirm the deterioration of the material in this temperature range.

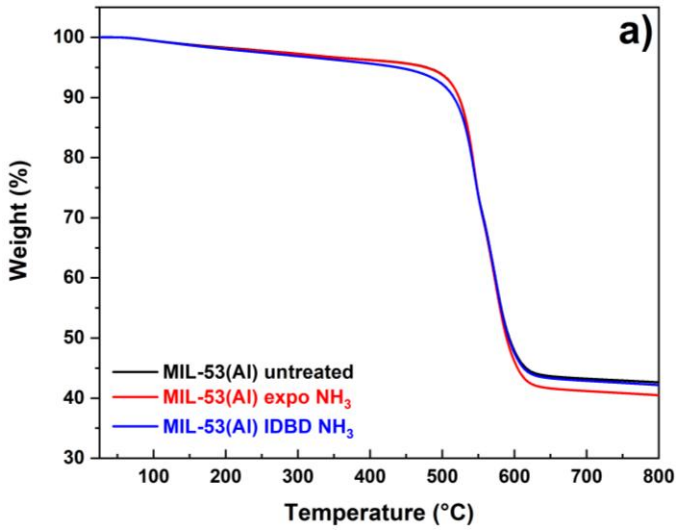

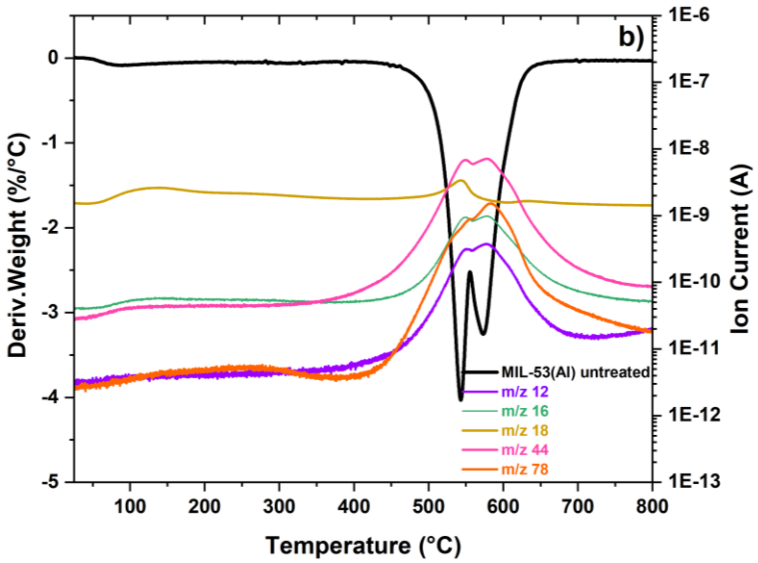

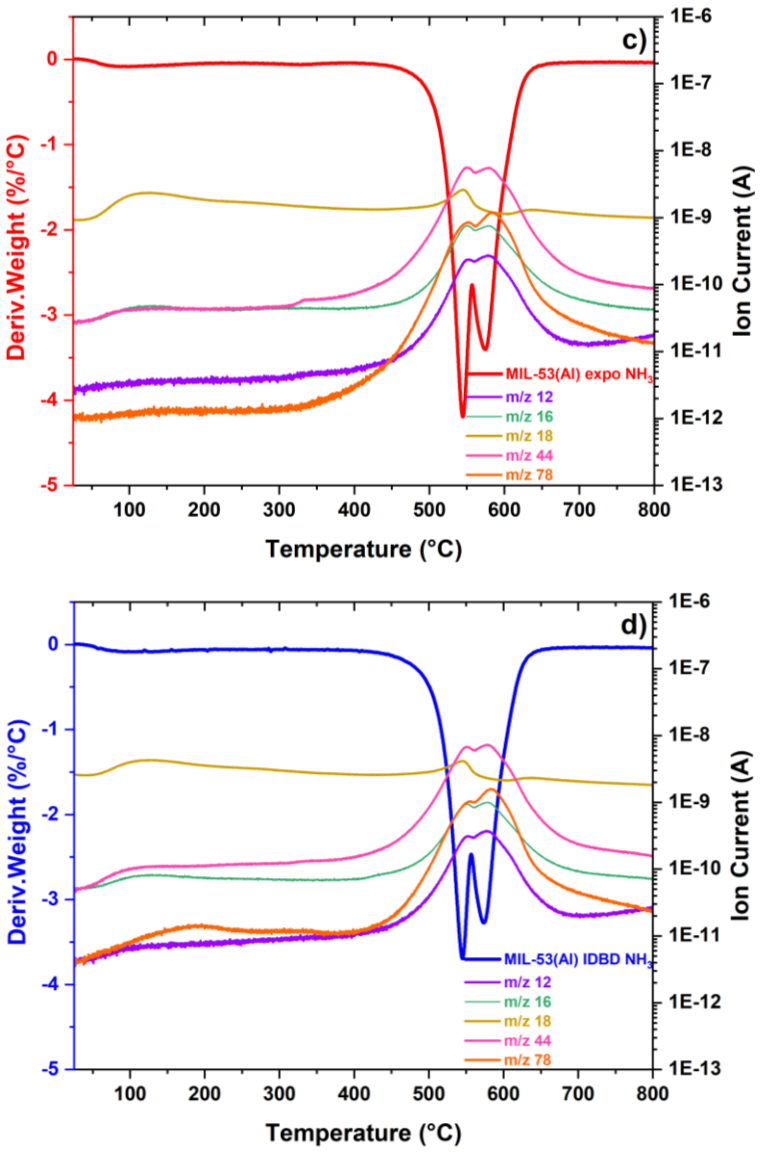

Figure 5. *(a) TGA curves of pristine MIL-53(Al), MIL-53(Al) exposed in NH_3 and MIL-53(Al) treated by IDBD in NH_3, (b) DTG-MS curves of pristine MIL-53(Al), (c) DTG-MS curves of MIL-53(Al) exposed in NH_3, (d) DTG-MS curves of MIL-53(Al) treated by IDBD in NH_3*

3.5. XPS analysis

The surface chemical analysis by XPS of the three materials is presented in figure 6. The atomic percentage of the different chemical elements present in the three samples are reported in table S2 (supporting information). The C_{1s} spectrum of the untreated MIL-53(Al) (fig. 6.a) reveals two main

contributions, coming from the C-C (284.4 eV) and C(=O)-O (288.5 eV) moieties. Regarding MIL-53(Al) exposed in NH_3 (fig. 6.b) and MIL-53(Al) treated by IDBD in NH_3 (fig. 6.c), an obvious change in the chemical structure is observed in the C_{1s} spectrum. Three main contributions are observed: the first two correspond to C-C and C(=O)-O moieties, as it was for the pristine material, and the third contribution corresponds to the C-N (285.5 eV) bonds. For the O_{1s} spectra of the three samples, they show two main contributions: the first at 531 eV is attributed to the O-Al (O-metal) bonds, the second at 532 eV corresponds to the O=C moieties. As for the N_{1s} spectrum, since the chemical composition of the pristine MIL-53(Al) is devoid of nitrogen, we present only the N_{1s} spectra for MIL-53(Al) exposed in NH_3 and MIL-53(Al) treated by IDBD in NH_3. The N_{1s} spectrum of MIL-53(Al) exposed in NH_3 (fig. 6.g) shows a noisy signal with a poor signal to noise ratio, which suggests that there is quasi no nitrogen grafted on the material while in contact with ammonia. This seems to indicate that certain chemical reactions between MIL-53(Al) and ammonia gas could have taken place by simple contact. On the other hand, the N_{1s} spectrum of MIL-53(Al) treated by IDBD (fig. 6.h) reveals two contributions: a first one at 398.1 eV that is attributed to a pyridine-type bond, and a second contribution at 399.9 eV corresponding to N-C bonds. This result highlights a successful modification of the organic ligand of MIL-53(Al) by IDBD plasma treatment, by substitution of a carbon present in the benzene ring of terephthalic acid by a nitrogen to form a pyridine. It can thus be deduced that the exposure to NH_3 alone is insufficient to insert nitrogen in the MIL 53(Al) structure. On the other hand, the role of the plasma is decisive to insert nitrogen in the MOF structure.

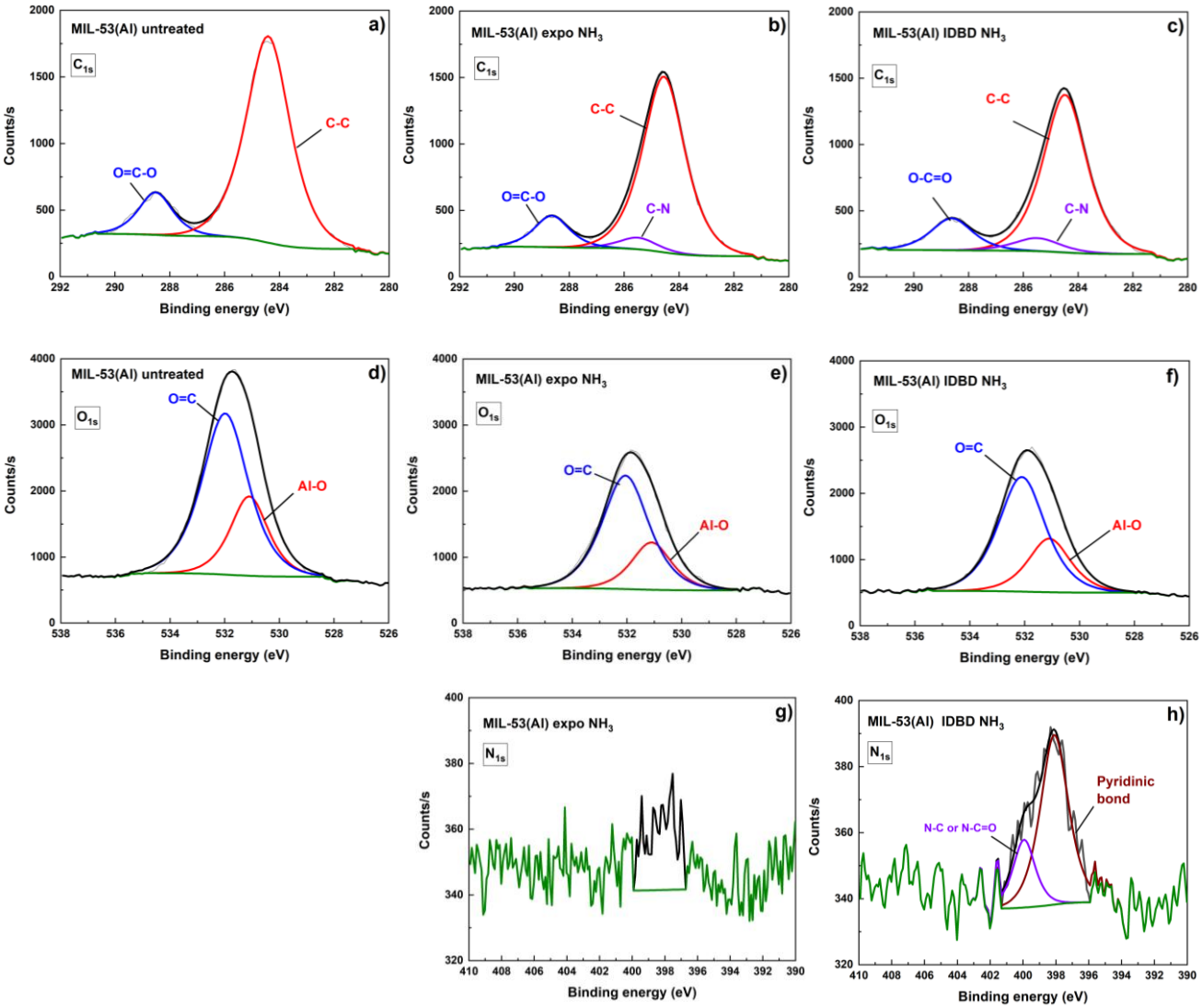

Figure 6. *C_{1s} spectra (a-c), O_{1s} spectra (d-f) and N_{1s} spectra (g,h) of pristine MIL-53(Al), MIL-53(Al) exposed in NH_3 and MIL-53(Al) treated by IDBD in NH_3.*

3.6. Textural properties

Figure 7.a shows the N_2 adsorption isotherms obtained at -196 °C on the three materials, all of them showed a significant N_2 uptake at very low relative pressure (P/P_0), below 10^{-3}, indicating an important fraction of microporosity (pores under 2 nm) [57] in the following order MIL-53(Al) expo NH_3 > MIL-53(Al) IDBD NH_3 > MIL-53(Al) untreated At P/P_0 between 0.1 and 0.85 there is not a plateau but a continuous N_2 uptake indicating the presence of large micropores and mesopores. The N_2 isotherm presents a change in slope from a relative pressure of 0.85, characteristic of capillary condensation.

The BET areas, A_{BET}, increased after the NH_3 treatments, from 410 $m^2.g^{-1}$ for MIL-53(Al) untreated, to 615 and 560 $m^2.g^{-1}$ for MIL-53(Al) expo NH_3 and MIL-53(Al) IDBD NH_3, respectively. $V_{0.97}$ followed the same tendency as A_{BET} and ranged from 0.45 to 0.55 $cm^3.g^{-1}$, for MIL-53(Al) untreated and MIL-53(Al) expo NH_3, respectively.

Although, the determination of the textural properties of porous materials is done mostly by N_2 adsorption at -196 °C. The IUPAC[58] recommends the use of Ar as a more suitable gas for surface and volume analysis of porous materials. Indeed, compared to the N_2 molecule, Ar has a spherical symmetry and so a null quadrupolar moment. Therefore, textural properties determination are not affected by specific interactions between Ar and the surface[51]. The adsorption of different gases, as N_2 and Ar, could be useful to evaluate specific interactions of these gases with the adsorbent surface. Figure 7b shows Ar adsorption isotherms at -186 °C on the three materials. If the shape of these isotherms is very similar to that of N_2 isotherms, the order of the adsorbed quantity of Ar at P/P_0 below 10^{-3} is this time greater in the case of untreated MIL-53(Al) than on MIL-53(Al) expo NH_3 and MIL-53(Al) IDBD NH_3. This fact shows that N_2 interact with N-fontionalities on the MOF surfaces and so N_2 uptake is not only due to texture but also to surface chemistry properties and should not be use to asess of the porosity. The A_{BET} was 680, 515 and 540 $m^2.g^{-1}$ for MIL-53(Al) untreated, MIL-53(Al) expo NH_3 and MIL-53(Al) IDBD NH_3, respectively. $V_{0.97}$ exhibited a contrasting trend compared to A_{BET}, the highest Ar uptake was observed in MIL-53(Al) expo NH_3 and the lowest in MIL-53(Al) untreated. A_{BET} primarily reflects microporosity, indicating that N-functionalization process reduces microporosity (pore diameter below 2 nm) in favor of mesoporosity (pore diameter between 2 and 50 nm) volume. The structural shrinkage of MOFs observed by XRD due to thermal effects may impact both micro and mesoporosity, leading to the merging of micropores and the formation of mesopores. The increase in total porosity, $V_{0.97}$, from 0.43 to 0.50-0.51 $cm^3.g^{-1}$ due to the treatments suggests that the structure could be partially damaged, and the removal of metallic ions and connectors cannot be excluded. Precisely determining micropore and mesopore volumes in MOFs is challenging, even when using Ar adsorption at 87K, as we did. Unlike carbons and zeolites, which have been studied for a long time, there are no Density Functional Theory (DFT) models specifically developed for each MOF that allow obtaining a pore size distribution (PSD). For this reason, and although the model developed for metal-exchanged zeolites provided by Micromeritics yielded logical tendencies for the microporosity, which decreased from 0.28 $cm^3.g^{-1}$ to 0.21-0.22 $cm^3.g^{-1}$, we decided not to present these results. This

decision is based on the fact that the model does not really consider the actual interactions between the hydrogen molecule and our MOF surfaces.

Table 1 shows A_{BET} and $V_{0.97}$ determined by N_2 and Ar adsorption for the three materials. Based on these results, it can be concluded that the sucessful N-functionalization achieved through NH_3 exposure appears to slightly decrease the microporosity of the material. However, this N-functionalization could have potential benefits for H_2 adsorption, as the molecule can be polarized similar to N_2.

Table 1. *BET areas and pore volume* at P/P_0=0.97 *of the untreated MIL-53(Al), MIL-53(Al) exposed in NH_3 and MIL-53(Al) treated by IDBD in NH_3 determined by N_2 and Ar adsorption isotherms at -196 and -186 °C, respectively*

MOF	N_2		Ar	
	$\mathbf{A_{BET}}$ [$m^2\ g^{-1}$]	$\mathbf{V_{0.97}}$ [$cm^3\ g^{-1}$]	$\mathbf{A_{BET}}$ [$m^2\ g^{-1}$]	$\mathbf{V_{0.97}}$ [$cm^3\ g^{-1}$]
MIL-53(Al) untreated	410	0.45	680	0.43
MIL-53(Al) expo NH_3	615	0.55	513	0.51
MIL-53(Al) IDBD NH_3	560	0.52	540	0.50

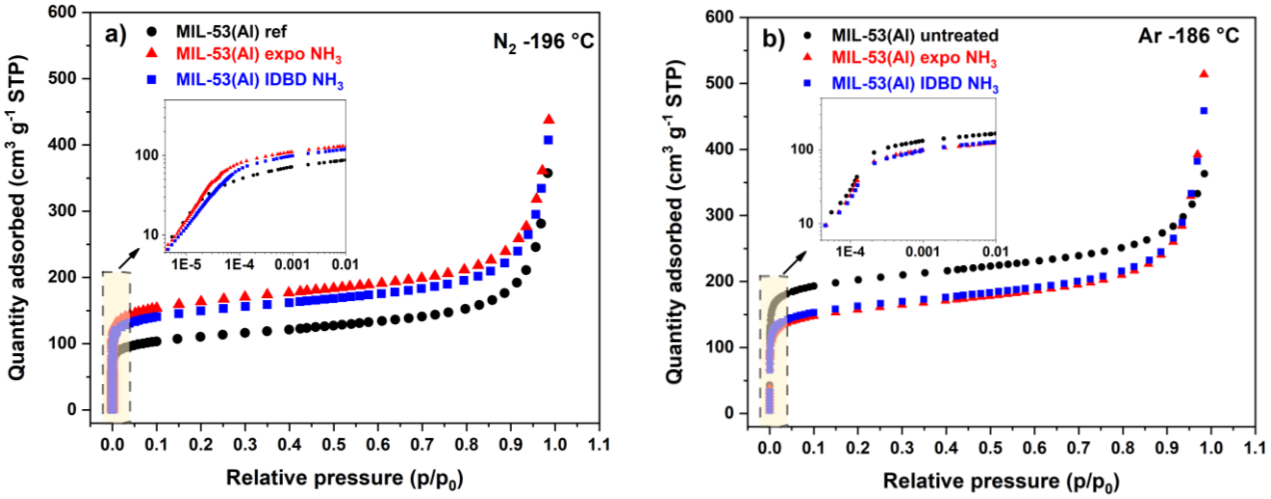

Figure 7. *(a) N_2 adsorption isotherms at -196 °C and (b) Ar adsorption isotherms at -186 °C on MIL-53(Al) ref MIL-53(Al) expo NH_3 and MIL-53(Al) IDBD NH_3, The insert in the figures shows the gaz uptake at relatives pressures under 0.1.*

3.7. H_2 adsorption capacities

Figure 8 shows the H_2 adsorption measurements up to 10^5 Pa at -196 °C (fig. 8.a) and 25 °C (fig. 8.b) for the 3 samples. H_2 adsorption capacity at -196 °C was greater for N-functionalized materials compared to the pristine MIL-53(Al) despite the reduction of the A_{BET} determined by Ar adsorption. This can be explained by the increase of specific interactions of the H_2 molecule with the N-functionalities. The H_2 adsorption capacity was 1.3 wt. % at 1 bar for the pristine MIL-53(Al), which is within the range reported in the literature[59-60]. At an absolute pressure of 5.10^4 Pa, H_2 absorbed was 0.9 wt.% for MIL-53(Al) untreated, and 1.0 wt.% for MIL-53(Al) expo NH_3 and MIL-53(Al) IDBD NH_3. Therefore, both functionalized materials showed an increase in H_2 uptake due to specific interactions. When increasing pressure up to 10^5 Pa, the H_2 adsorption capacities were 1.3 wt.% for MIL-53(Al) untreated and MIL-53(Al) IDBD NH_3. This can be attributed to the higher A_{BET} of MIL-53(Al) untreated, 680 $m^2.g^{-1}$, compared to MIL-53(Al) IDBD NH_3, 550 $m^2.g^{-1}$ after plasma treatment, as measured by Ar adsorption. Nevertheless, the H_2 adsorption capacity at 10^5 Pa remains higher for MIL-53(Al) expo NH_3, reaching 1.4 wt.%, despite having the lowest A_{BET} measured by Ar adsorption, 515 $m^2.g^{-1}$. This is attributed to stronger interactions between the H_2 molecule and this material, which

is confirmed by the fact that the A_{BET} measured by N_2 adsorption is the highest for this material. Both N_2 and H_2 have a quadrupolar moment, making them sensitive to the chemical composition of the surface. Figure 8.b shows H_2 adsorption at 25 °C for the three materials, the adsorbed quantities were much lower and uncertainties in these measurements could be important, especially for MIL-53(Al) expo NH_3. MIL-53(Al) IDBD NH_3 showed the best performance at 25 °C, obtaining an increase of ~ 50 % of the H_2 storage capacity compared to MIL-53(Al) untreated. The adsorbed quantities at 25 °C are low when compared to the results obtained at -196 °C but remain promising in the context of this study and for an optimization of MIL-53(Al) in use under environmental conditions of pressure and temperature.

The presented results have successfully validated the effectiveness of plasma treatment in grafting N-functionalities within the structure of MIL-53(Al). Moreover, this study paves the way for future research opportunities, particularly in the area of H_2 storage.

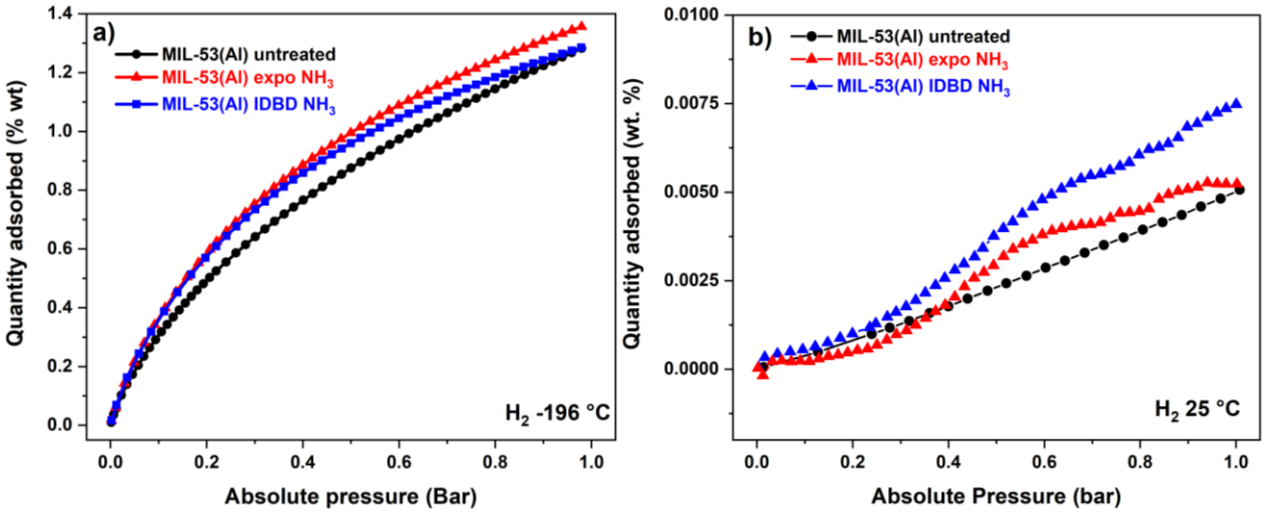

Figure 8. *(a) H_2 adsorption isotherms at -196 °C and (b) 25 °C on MIL-53(Al) untreated, MIL-53(Al) expo NH_3 and MIL-53(Al) IDBD NH_3,*

4. Conclusion

This study focuses on the functionalization process of MIL-53(Al) using impulse dielectric barrier discharge (IDBD) plasma treatment under an NH_3 atmosphere. The results confirmed the effectiveness of the IDBD treatment in grafting N-groups onto the organic linker of MIL-53(Al). Plasma diagnostics and optical measurements revealed successful functionalization without material deterioration and

high-temperature X-ray diffraction patterns indicated good chemical stability against ammonia and maintained crystalline structure up to 450 °C. XPS analysis confirmed the presence of nitrogen in the treated material, validating the successful functionalization. Additionally, the study showed an approximately 50% increase in hydrogen storage capacity for MIL-53(Al) treated with IDBD, promising the development of materials with higher adsorption capacities at room temperature and atmospheric pressure. These outcomes highlight the potential of IDBD plasma treatment for N-functionalization and pave the way for further research in functionalizing other metal-organic frameworks and enhancing gas adsorption applications.

Funding

This work has been funded by the French Research Agency (ANR) under SYNERGY project (ANR-20-CE05-0013) and SOLHYD project (ANR-22-PEHY-0007). This study was partially supported by the TALiSMAN and TALiSMAN2 projects funded by the European Regional Development Fund (ERDF), and HyPE project (FRCR program funded by Région Grand-Est and FEDER).

References

[1] B. Li, H.-M. Wen, Y. Cui, W. Zhou, G. Qian, B. Chen, Emerging Multifunctional Metal–Organic Framework Materials. Adv. Mater. 28 (2016) 8819–8860

https://doi.org/10.1002/adma.201601133

[2] H.-C. Zhou, J.R. Long, O.M. Yaghi, Introduction to Metal–Organic Frameworks, Chem. Rev. 112 (2012) 673–674.

https://doi.org/10.1021/cr300014x.

[3] Y. Wu, Y. Li, J. Gao, Q. Zhang, Recent advances in vacancy engineering of metal- organic frameworks and their derivatives for electrocatalysis, SusMat. 1 (2021) 66–87.

https://doi.org/10.1002/sus2.3.

[4] A.E. Baumann, D.A. Burns, B. Liu, V.S. Thoi, Metal-organic framework functionalization and design strategies for advanced electrochemical energy storage devices, Commun Chem. 2 (2019) 86. https://doi.org/10.1038/s42004-019-0184-6.

[5] N. Ullah, S. Ullah, S. Khan, D. Guziejewski, V. Mirceski, A review: Metal-organic framework based electrocatalysts for methanol electro-oxidation reaction, International Journal of Hydrogen Energy 48 (2023) 3340–3354.

https://doi.org/10.1016/j.ijhydene.2022.10.200.

[6] J.P. Marco-Lozar, J. Juan-Juan, F. Suárez-García, D. Cazorla-Amorós, A. Linares-Solano, MOF-5 and activated carbons as adsorbents for gas storage, International Journal of Hydrogen Energy. 37 (2012) 2370–2381. https://doi.org/10.1016/j.ijhydene.2011.11.023.

[7] S. Yu, G. Jing, S. Li, Z. Li, X. Ju, Tuning the hydrogen storage properties of MOF-650: A combined DFT and GCMC simulations study, International Journal of Hydrogen Energy. 45 (2020) 6757–6764. https://doi.org/10.1016/j.ijhydene.2019.12.114.

[8] J. Ren, H.W. Langmi, B.C. North, M. Mathe, D. Bessarabov, Modulated synthesis of zirconium-metal organic framework (Zr-MOF) for hydrogen storage applications, International Journal of Hydrogen Energy. 39 (2014) 890–895.

https://doi.org/10.1016/j.ijhydene.2013.10.087.

[9] S.J. Alesaadi, F. Sabzi, Hydrogen storage in a series of Zn-based MOFs studied by Sanchez–Lacombe equation of state, International Journal of Hydrogen Energy. 40 (2015) 1651-1656.

https://doi.org/10.1016/j.ijhydene.2014.12.008.

[10] S. Rostami, A. Nakhaei Pour, A. Salimi, A. Abolghasempour, Hydrogen adsorption in metal- organic frameworks (MOFs): Effects of adsorbent architecture, International Journal of Hydrogen Energy 43 (2018) 7072–7080.

https://doi.org/10.1016/j.ijhydene.2018.02.160.

[11] M.S. Alhumaimess, Metal–organic frameworks and their catalytic applications, Journal of Saudi Chemical Society. 24 (2020) 461–473.

https://doi.org/10.1016/j.jscs.2020.04.002.

[12] Y. Chen, Z. Yang, H. Hu, X. Zhou, F. You, C. Yao, F.J. Liu, P. Yu, D. Wu, J. Yao, R. Hu, X. Jiang, H. Yang, Advanced Metal–Organic Frameworks-Based Catalysts in Electrochemical Sensors, Front. Chem. 10 (2022) 881172.

https://doi.org/10.3389/fchem.2022.881172.

[13] B.-L. Xiang, L. Fu, Y. Li, Y. Liu, Preparation of Fe(II)/MOF-5 Catalyst for Highly Selective Catalytic Hydroxylation of Phenol by Equivalent Loading at Room Temperature, Journal of Chemistry. 2019 (2019) 1–10. https://doi.org/10.1155/2019/8950630.

[14] C. Chen, J. Li, Z. Lv, M. Wang, J. Dang, Recent strategies to improve the catalytic activity of pristine MOFs and their derived catalysts in electrochemical water splitting, International Journal of Hydrogen Energy. 48 (2023) 30435-30463.

https://doi.org/10.1016/j.ijhydene.2023.04.241.

[15] H.D. Lawson, S.P. Walton, C. Chan, Metal–Organic Frameworks for Drug Delivery: A Design Perspective, ACS Applied Materials & Interfaces. 13 (2021) 7004–7020. https://doi.org/10.1021/acsami.1c01089.

[16] S. He, L. Wu, X. Li, H. Sun, T. Xiong, J. Liu, C. Huang, H. Xu, H. Sun, W. Chen, R. Gref, J. Zhang, Metal-organic frameworks for advanced drug delivery, Acta Pharmaceutica Sinica B. 11 (2021) 2362–2395. https://doi.org/10.1016/j.apsb.2021.03.019.

[17] Y. Sun, L. Zheng, Y. Yang, X. Qian, T. Fu, X. Li, Z. Yang, H. Yan, C. Cui, W. Tan, Metal–Organic Framework Nanocarriers for Drug Delivery in Biomedical Applications, Nano-Micro Lett. 12 (2020) 103. https://doi.org/10.1007/s40820-020-00423-3.

[18] T. Qiu, Z. Liang, W. Guo, H. Tabassum, S. Gao, R. Zou, Metal–Organic Framework-Based Materials for Energy Conversion and Storage, ACS Energy Lett. 5 (2020) 520–532. https://doi.org/10.1021/acsenergylett.9b02625.

[19] Y. Zhao, Z. Song, X. Li, Q. Sun, N. Cheng, S. Lawes, X. Sun, Metal organic frameworks for energy storage and conversion, Energy Storage Materials. 2 (2016) 35–62. https://doi.org/10.1016/j.ensm.2015.11.005.

[20] C. Pettinari, A. Tombesi, MOFs for Electrochemical Energy Conversion and Storage, Inorganics. 11 (2023) 65.

https://doi.org/10.3390/inorganics11020065.

[21] W. Wang, D. Chen, F. Li, X. Xiao, Q. Xu, Metal-organic-framework-based materials as platforms for energy applications, Chem 10 (2024) 86–133.

https://doi.org/10.1016/j.chempr.2023.09.009.

[22] K. Suresh, D. Aulakh, J. Purewal, D.J. Siegel, M. Veenstra, A.J. Matzger, Optimizing Hydrogen Storage in MOFs through Engineering of Crystal Morphology and Control of Crystal Size, Journal of the American Chemical Society. 143 (2021) 10727–10734.

https://doi.org/10.1021/jacs.1c04926.

[23] D. Zhao, X. Wang, L. Yue, Y. He, B. Chen, Porous metal–organic frameworks for hydrogen storage, Chem. Commun. 58 (2022) 11059–11078.

https://doi.org/10.1039/D2CC04036K.

[24] A.M.P. Peedikakkal, I.H. Aljundi, Upgrading the Hydrogen Storage of MOF-5 by Post-Synthetic Exchange with Divalent Metal Ions, Applied Sciences. 11 (2021) 11687.

https://doi.org/10.3390/app112411687.

[25] M. El Kassaoui, M. Lakhal, A. Benyoussef, A. El Kenz, M. Loulidi, Enhancement of hydrogen storage properties of metal-organic framework-5 by substitution (Zn, Cd and Mg) and decoration (Li, Be and Na), International Journal of Hydrogen Energy 46 (2021) 26426–26436. https://doi.org/10.1016/j.ijhydene.2021.05.107.

[26] R.M. Kumar, J.V. Sundar, V. Subramanian, Improving the hydrogen storage capacity of metal organic framework by chemical functionalization, International Journal of Hydrogen Energy 37 (2012) 16070–16077. https://doi.org/10.1016/j.ijhydene.2012.08.052.

[27] J. Park, Z.U. Wang, L.-B. Sun, Y.-P. Chen, H.-C. Zhou, Introduction of Functionalized Mesopores to Metal–Organic Frameworks via Metal–Ligand–Fragment Coassembly, Journal of the American Chemical Society. 134 (2012) 20110–20116.

https://doi.org/10.1021/ja3085884.

[28] O.M. Yaghi, M.J Kalmutzki, C.S Diercks, Functionalization of MOFs, in: Introduction to Reticular Chemistry, John Wiley & Sons, Ltd, 2019: pp. 145–176.

https://doi.org/10.1002/9783527821099.ch6.

[29] E.M. Thoresen, S. Øien-Ødegaard, G. Kaur, M. Tilset, K.P. Lillerud, M. Amedjkouh, Strongly visible light-absorbing metal–organic frameworks functionalized by cyclometalated ruthenium(ii) complexes, RSC Adv. 10 (2020) 9052–9062.

https://doi.org/10.1039/C9RA06984D.

[30] S. Mandal, S. Natarajan, P. Mani, A. Pankajakshan, Post-Synthetic Modification of Metal–Organic Frameworks Toward Applications, Advanced Functional Materials. 31 (2021) 2006291. https://doi.org/10.1002/adfm.202006291.

[31] L. Xia, Q. Liu, F. Wang, J. Lu, Improving the hydrogen storage properties of metal-organic framework by functionalization, Journal of Molecular Modeling. 22 (2016) 254.

https://doi.org/10.1007/s00894-016-3129-3.

[32] W. Fan, X. Wang, B. Xu, Y. Wang, D. Liu, M. Zhang, Y. Shang, F. Dai, L. Zhang, D. Sun, Amino-functionalized MOFs with high physicochemical stability for efficient gas storage/separation, dye adsorption and catalytic performance, J. Mater. Chem. A. 6 (2018) 24486–24495. https://doi.org/10.1039/C8TA07839D.

[33] Y.-B. Zhang, H. Furukawa, N. Ko, W. Nie, H.J. Park, S. Okajima, K.E. Cordova, H. Deng, J. Kim, O.M. Yaghi, Introduction of Functionality, Selection of Topology, and Enhancement of Gas Adsorption in Multivariate Metal–Organic Framework-177, Journal of the American Chemical Society. 137 (2015) 2641–2650.

https://doi.org/10.1021/ja512311a.

[34] A. Najah, D. Boivin, C. Noël, L. De Poucques, G. Henrion, S. Cuynet, Amino-grafting pre-functionalization of terephthalic acid by impulse dielectric-barrier discharge (DBD) plasma for amino-based Metal-Organic Frameworks (MOFs), Materials Chemistry and Physics. 290 (2022) 126629. https://doi.org/10.1016/j.matchemphys.2022.126629.

[35] P. Dimitrakellis, F. Faubert, M. Wartel, E. Gogolides, S. Pellerin, Plasma Surface Modification of Epoxy Polymer in Air DBD and Gliding Arc, Processes. 10 (2022) 104. https://doi.org/10.3390/pr10010104.

[36] H. Turkoglu Sasmazel, M. Alazzawi, N. Kadim Abid Alsahib, Atmospheric Pressure Plasma Surface Treatment of Polymers and Influence on Cell Cultivation, Molecules. 26 (2021) 1665. https://doi.org/10.3390/molecules26061665.

[37] S. Yoshida, K. Hagiwara, T. Hasebe, A. Hotta, Surface modification of polymers by plasma treatments for the enhancement of biocompatibility and controlled drug release, Surface and Coatings Technology. 233 (2013) 99–107.

https://doi.org/10.1016/j.surfcoat.2013.02.042.

[38] K.V. Rani, B. Sarma, A. Sarma, Plasma treatment on cotton fabrics to enhance the adhesion of Reduced Graphene Oxide for electro-conductive properties, Diamond and Related Materials. 84 (2018) 77–85. https://doi.org/10.1016/j.diamond.2018.03.009.

[39] M. Ayesh, A.R. Horrocks, B.K. Kandola, The Impact of Atmospheric Plasma/UV Laser Treatment on the Chemical and Physical Properties of Cotton and Polyester Fabrics, Fibers. 10 (2022) 66. https://doi.org/10.3390/fib10080066.

[40] A.I. Susan, M. Widodo, M. Nur, Corona Glow Discharge Plasma Treatment for Hidrophylicity Improvement of Polyester and Cotton Fabrics, IOP Conf. Ser.: Mater. Sci. Eng. 214 (2017) 012031. https://doi.org/10.1088/1757-899X/214/1/012031.

[41] Y. Lin, H. Li, Q. Wang, Z. Gong, J. Tao, Effect of plasma surface treatment of aluminum alloy sheet on the properties of Al/Gf/PP laminates, Applied Surface Science. 507 (2020) 145062. https://doi.org/10.1016/j.apsusc.2019.145062.

[42] F. Widdascheck, M. Kothe, A.A. Hauke, G. Witte, The effect of oxygen plasma treatment of gold electrodes on the molecular orientation of CuPc films, Applied Surface Science. 507 (2020) 145039. https://doi.org/10.1016/j.apsusc.2019.145039.

[43] D.F. Williams, E.J.C. Kellar, D.A. Jesson, J.F. Watts, Surface analysis of 316 stainless steel treated with cold atmospheric plasma, Applied Surface Science. 403 (2017) 240–247. https://doi.org/10.1016/j.apsusc.2017.01.150.

[44] A. Boutin, M.-A. Springuel-Huet, A. Nossov, A. Gédéon, T. Loiseau, C. Volkringer, G. Férey, F.-X. Coudert, A.H. Fuchs, Breathing Transitions in MIL-53(Al) Metal-Organic Framework Upon Xenon Adsorption, Angewandte Chemie International Edition. 48 (2009) 8314–8317. https://doi.org/10.1002/anie.200903153.

[45] A. Ghoufi, K. Benhamed, L. Boukli-Hacene, G. Maurin, Electrically Induced Breathing of the MIL-53(Cr) Metal–Organic Framework, ACS Central Science. 3 (2017) 394–398. https://doi.org/10.1021/acscentsci.6b00392.

[46] J. Bitzer, S.-L. Heck, W. Kleist, Tailoring the breathing behavior of functionalized MIL-53(Al,M)-NH2 materials by using the mixed-metal concept, Microporous and Mesoporous Materials. 308 (2020) 110329.

https://doi.org/10.1016/j.micromeso.2020.110329.

[47] O. Weser, V. Veryazov, In Search of the Reason for the Breathing Effect of MIL53 Metal-Organic Framework: An ab Initio Multiconfigurational Study, Front. Chem. 5 (2017) 111. https://doi.org/10.3389/fchem.2017.00111.

[48] T. Loiseau, C. Serre, C. Huguenard, G. Fink, F. Taulelle, M. Henry, T. Bataille, G. Férey, A Rationale for the Large Breathing of the Porous Aluminum Terephthalate (MIL-53) Upon Hydration, Chemistry – A European Journal. 10 (2004) 1373–1382.

https://doi.org/10.1002/chem.200305413.

[49] Powder diffraction file database (PDF-4)

www.icdd.com/pdf-4/

[50] CasaXPS Database.

www.casaxps.com.

[51] J. Rouquerol, F. Rouquerol, K. Sing, Adsorption by powder and porous solids. Principles, methodology and applications (1999)

ISBN: 978-0-12-598920-6

[52] J. Jagiello, J. Kenvin, A. Celzard, V. Fierro, Enhanced resolution of ultra micropore size determination of biochars and activated carbons by dual gas analysis using N2 and CO2 with 2D-NLDFT adsorption models, Carbon 144 (2019) 206–215.

https://doi.org/10.1016/j.carbon.2018.12.028.

[53] J. Jagiello, J. Kenvin, C.O. Ania, J.B. Parra, A. Celzard, V. Fierro, Exploiting the adsorption of simple gases O2 and H2 with minimal quadrupole moments for the dual gas characterization of nanoporous carbons using 2D-NLDFT models, Carbon. 160 (2020) 164–175.

https://doi.org/10.1016/j.carbon.2020.01.013.

[54] Watson, J. K. G.; Majewski, W. A.; Glownia, J. H. Assignment of the Schuster Band of Ammonia. Journal of Molecular Spectroscopy 1986, 115 (1), 82–87.

https://doi.org/10.1016/0022-2852(86)90277-8.

[55] L. Silvester, A. Naim, A. Fateeva, G. Postole, A. Auroux, L. Massin, P. Gelin, L. Bois, Fine tuning of the physico-chemical properties of a MIL-53(Al) type - Mesoporous alumina composite using a facile sacrificial-template synthesis approach, Microporous Mesoporous Mater. 306 (2020) 110443.

https://doi.org/10.1016/j.micromeso.2020.110443.

[56] L. Feng, R. Chen, S. Hou, W. Chen, H. Huang, Y. Wang, Y. Wu, F. Li, Common but differentiated flexible MIL-53(Al): role of metal sources in synthetic protocol for tuning the adsorption characteristics, J Mater Sci. 54 (2019) 6174–6185.

https://doi.org/10.1007/s10853-018-03287-6.

[57] J. Rouquerol, D. Avnir, C.W. Fairbridge, D.H. Everett, J.H. Haynes, N. Pernicone, J.D.F. Ramsay, K.S.W. Sing, K.K. Unger, *Recommendations for the Characterization of Porous Solids*, Pure Appl. Chem. 68 (1994) 1739-1758
https://doi.org/10.1515/iupac.66.0925.

[58] M. Thommes, K. Kaneko, A.V. Neimark, J.P. Olivier, F. Rodriguez-Reinoso, J. Rouquerol, K.S.W. Sing, Physisorption of gases, with special reference to the evaluation of surface area and pore size distribution (IUPAC Technical Report), Pure Appl. Chem. 87 (2015) 1051–1069.

https://doi.org/10.1515/pac-2014-1117.

[59] G. Férey, M. Latroche, C. Serre, F. Millange, T. Loiseau, A. Percheron-Guégan, Hydrogen adsorption in the nanoporous metal-benzenedicarboxylate M(OH)(O2C–C6H4–CO2) (M = Al3+, Cr3+), MIL-53, Chem. Commun. (2003) 2976–2977

https://doi.org/10.1039/B308903G.

[60] D. Himsl, D. Wallacher, M. Hartmann, Improving the Hydrogen-Adsorption Properties of a Hydroxy-Modified MIL-53(Al) Structural Analogue by Lithium Doping, Angew. Chem. Int. Ed. 48 (2009) 4639–4642.

https://doi.org/10.1002/anie.200806203